CHAPTER IV

POLYMER–SURFACTANT COMPLEX FORMATION AND ITS EFFECT ON TURBULENT WALL SHEAR STRESS

4.1 Abstract

Turbulent drag reduction in Couette flow was investigated in terms of a decrease in wall shear stress for aqueous solutions of a nonionic polymer, poly(ethylene oxide) (PEO), a cationic surfactant, hexadecyltrimethylammonium choride (HTAC), and their mixtures. Consistent with literature data, drag reduction was observed for PEO solutions above a critical molecular weight, $0.91 \times 10^5 < M_c < 3.04 \times 10^5$. Maximum drag reduction occurred at an optimum concentration, c^*_{PEO}, which scales inversely with molecular weight, and the % maximum drag reduction increases with molecular weight. For aqueous HTAC solutions, wall shear stress decreased with increasing HTAC concentration and leveled off at an optimum concentration, c^*_{HTAC}, comparable to the critical micelle concentration. For HTAC/PEO mixtures, the critical PEO molecular weight for drag reduction decreases. At fixed PEO concentration, maximum drag reduction was observed at an optimum HTAC concentration, $c^*_{HTAC/PEO}$, comparable to the maximum binding concentration, MBC. Also, with HTAC concentration fixed at the MBC, the optimum PEO concentration for drag reduction, $c^*_{PEO/HTAC}$, decreases relative to that, c^*_{PEO}, in the absence of HTAC. These observations are consistent with previous studies which showed that the hydrodynamic volume of PEO increases because of electrostatic repulsions between bound HTAC micelles and reaches a maximum value at the MBC.

4.2 Introduction

Turbulent drag reduction, DR, is a flow phenomenon in which a small amount of additive induces a drastic reduction of skin friction in turbulent flow. This phenomenon is important to a variety of applications; crude oil transport, fire

fighting, waste water management, transport of solids in water and heating circuits, hydraulic and jet machinery, and in biomedical studies [1,2,3,4,5]. DR has been investigated extensively with regard to variables, such as type of drag reducing additive, additive concentration, molecular weight, additive structure, temperature, and solvent quality [6,7,8].

Several theories have been proposed to describe the mechanism of drag reduction. The general consensus is that energy dissipation via macromolecular extension is involved in the mechanism of drag reduction (Virk [9]). Hlavacek et al. [10] proposed that, a macromolecule can suppress turbulence by pervading two or more microdisturbanmces or turbulence precursors, hindering their free movement and growth. Lumley [11-13] suggested that the macromolecules become expanded due to the fluctuating strain rate in the turbulent zone outside the laminar sublayer close to the wall. The macromolecular expansion yields a dramatic increase in viscosity which results in a thickening of the viscous sublayer, where the viscosity remains unchanged because coils are unstretched. This reduces the velocity gradient at the wall and hence leads to a reduction of the drag. The idea that drag reduction originates in large viscosity increases in the turbulent zone was criticized by De Gennes [14,15], on the basis that the chains stretch affinely in the fluid elements, and he proposed instead that the partially-stretched polymer molecules elastically store the kinetic energy of turbulent eddies. More recently, Ryskin [16] presented a new argument that drag reduction stems from a viscosity increases, on the basis that, above a critical strain rate, the polymer chain does not deform affinely, but unravels like a yo-yo such that the central portion remains taut, while the end portions remain coiled. When the flow becomes weak, the polymer chain retracts into a fully-coiled state. The taut central portion generates a large stress and facilitates viscous dissipation of turbulent kinetic energy. Thus, although, DR was discovered over fifty years ago [17], a complete theoretical understanding, encompassing all types of drag reducers, has not been established, and DR remains an important topic for further investigation.

The most effective drag-reducing polymers, in general, possess a linear flexible structure and very high molecular weight. Poly(ethylene oxide), PEO, which is commercially available in a wide range of molecular weights, is known to be

suitable for use as a drag reducer [18]. However, drag-reducing polymers are sensitive to mechanical and thermal degradation. In the last decade, there has been a great deal of interest in aqueous surfactant drag-reducing systems [19,20] as a class of additives which are self-repairable after degradation, making them suitable for potential applications in recirculating systems. Among the drag reducing surfactants, the cationic species (hexadecyltrimethyl ammonium chloride, HTAC) has been shown to be an effective drag reducer [21,22,23], when used in combination with organic salts such as sodium salicylate, which facilitates the formation of wormlike micellar structures.

Recent studies have demonstrated that water-soluble polymers like PEO form complexes with cationic surfactants such as HTAC [24,25] in which surfactant micelles are bound to the polymer. The formation of such complexes causes characteristic changes in solution viscosity, because of the increased hydrodynamic volume of the complex. Specifically, the reduced specific viscosity of a dilute aqueous PEO solution increases on titration with HTAC up to a maximum value, which corresponds to the maximum binding point, and then decreases due to screening of the electrostatic repulsions between bound micelles by excess added HTAC [24,25]. Similar behavior was observed in the radius of gyration and hydrodynamic radius measured by static and dynamic light scattering experiments [24,25]. These observations motivate the present study, to investigate whether such complex formation survives in turbulent flow conditions, and hence produces a synergistic response in the drag reduction characteristics of PEO and HTAC. Thus, we compare drag reduction behaviors of PEO, HTAC, and their mixtures in dilute aqueous solution. We seek to establish correlations between drag reduction effectiveness, PEO molecular weight, and HTAC concentration.

4.3 Experimental

4.3.1 Materials

Nonionic water soluble, poly(ethylene oxide), PEO, with quoted average molecular weights of 1.0×10^5, 3.0×10^5, 6.0×10^5, 9.0×10^5 and 4.0×10^6 g/mol (Aldrich

Chemical Co.) was used as received. Hexadecyl trimethylammonium choride ($C_{16}H_{33}N(CH_3)_3Cl$), HTAC, obtained from Unilever Thai Holdings, Ltd was used without further purification. This product contains 50% active surfactant, 36% water and 14 % isopropyl alcohol. The molecular weight of HTAC is 319.5 g/mol. Distilled water was used as a solvent after being twice filtered through 0.22 μm cellulose acetate Millipore membranes.

4.3.2 Sample Preparation

PEO stock solutions of 0.5 %(w/v) were prepared and stirred gently at room temperature for 4 to 30 days, depending on polymer molecular weight. For light scattering measurements, sample solutions, obtained by dilution of the stock solution, were centrifuged at 10,000 rpm for 15 minutes and then filtered through 0.22, 0.45 or 0.80 μm cellulose acetate Millipore membranes, depending on the concentration and molecular weight of the polymer, to remove suspended dust particles and impurities.

4.3.3 Instrumentation

Kinematic viscosity measurements were carried out using a Cannon-Ubbelohde viscometer (size no. 50, with ± 0.2% precision) at 30°C. The measured efflux times were converted to reduced viscosity and specific viscosity, neglecting the density difference between solution and solvent ($\rho_{water\ 30^oC} = 0.9957\ g/cm^3$). The intrinsic viscosity was determined using Huggins and Kramer plots, and the viscosity-average molecular weight was computed via the Mark – Houwink - Sakurada equation with $K = 1.25 \times 10^{-4}$ dL/g and $a = 0.75$ [26].

Dynamic and static light scattering measurements, DLS and SLS, (Malvern Instruments Company, model 4700) were made using an argon laser emitting vertically polarized light at wavelength of 514.5 nm. DLS was used to determine the apparent z-average diffusion coefficient, $\langle D_{app} \rangle$, at different scattering angles θ, and the center of mass diffusion coefficient, D_{cm}, of the polymer chain was then obtained by extrapolation of $\langle D_{app} \rangle$ to zero scattering angle based on the following equation:

$$<D_{app}>=D_{cm}(1+ q^2R_g^2 +...) \quad [4.1]$$

where C is a coefficient determined by the slowest internal mode of motion of the particle and by the size, flexibility, and polydispersity of the polymer [27]. R_g is the radius of gyration of the polymer chain. The diffusion coefficient at infinite dilution, D_o, was obtained by extrapolation of D_{cm} to zero polymer concentration, c_p (g/l), using the following equation.

$$D_{cm} = D_o (1 + k_D c_p + ...) \quad [4.2]$$

where k_D (l/g) is defined as the concentration dependence of D_{cm} (m^2/s) due to thermodynamic and hydrodynamic interactions. The hydrodynamic radius was calculated from D_o (m^2/s) using the well-known Stokes-Einstein equation:

$$R_h = k_B T/6\pi\eta_s D_o \quad [4.3]$$

where k_B is Boltzmann's constant (N.m/K), T is absolute temperature (K) and η_s is the viscosity of solvent (kg/m.s).

Static light scattering data were analyzed and interpreted by the Zimm-Debye equation. In the small-angle limit, this can be expressed as:

$$(Kc/\Delta R_\theta) = (1/M_w)(1 + (q^2R_g^2)/3) + 2A_2c \quad [4.4]$$

where M_w is the weight-average molecular weight, A_2 is the second virial coefficient, R_g^2 is the z-average of the mean square radius of gyration, ΔR_θ indicates the excess Rayleigh ratio, calculated from the excess scattering from the solution relative to a standard fluid:

$$\Delta R_\theta = ((\Delta I_{\theta(solution)}/I_{\theta(standard)}) \times R_{\theta(standard)} \times (n^2_{(solution)}/n^2_{(standard)})) \quad [4.5]$$

Here $\Delta I_{\theta(solution)}$ is the excess scattered intensity of the sample solution relative to the solvent; $n_{(solution)}$ and $n_{(standard)}$ are the refractive indices of the sample solution and standard fluid. K is the optical constant:

$$K = 4\pi^2 n^2 (dn/dc)^2 / N_A \lambda^4 \quad [4.6]$$

where n is the refractive index of the solvent, c is the polymer concentration (g/cm^3), λ is the wavelength of incident light (514.5 nm), dn/dc is the refractive index increment (cm^3/g), N_A is the Avogadro's number, and q is the scattering wave vector (cm^{-2}). In the SLS measurement, toluene (AR grade, Lab-Scan) was used as a standard solution with the Rayleigh ratio of 3.2×10^{-5} cm^{-1}.

A Du-Nouy ring tensiometer with Pt-plate, RI 10 probe (Kruss, model K 10T) was used to determine the surface tension of polymer and surfactant solutions.

A conductivity meter (Orion Co., model 160) was used to determine the electrical conductivity of polymer and surfactant solutions.

A fluids rheometer (Rheometrics, model ARES V6.5.6) was used to investigate turbulent wall shear stresses of PEO and HTAC solutions and their mixtures. The experiment was carried out using two Couette cells: a single couette cell (SCU), and a double couette cell (DCU). The single couette cell had a cup diameter of 47.9 mm and a bob diameter of 40.0 mm. For the double couette cell, the diameter of the outer cup and outer bob were identical to those of the single couette cell, whereas the inner cup and inner bob diameters were R_{IC} = 14.4 and R_{IB} = 36.1 mm, respectively. The bob length, L, was 40.0 mm and the gap between the upper bob and the lower cup was set at 0.05 mm. The temperature was controlled by a water bath controller at 30.0 ± 1.0 °C. The torque was measured by a transducer connected to the upper bob.

The inner wall shear stress, τ_w (N/m^2), of the samples was computed as the difference between the total torque measured by the DCU and the torque measured by the SCU according to the following equation:

$$\tau_w = (M_{DCU} - M_{SCU})K_\tau \quad [4.7]$$

where M_{DCU} (N.m) is the total DCU torque and M_{SCU} is the SCU torque, and K_τ (m^{-3}) is a stress constant, which can be expressd as

$$K_\tau = 1/2\pi L(R_{IB})^2 \quad [4.8]$$

where L is the bob length (m) and R_{IB} is the inner radius of the bob (m).

The inner shear strain rate was calculated from the relation

$$\dot{\gamma} = \theta K_\gamma \quad [4.9]$$

where $\dot{\gamma}$ is shear rate (s^{-1}), θ is the angular velocity (s^{-1}) and K_γ is a strain constant which can be expressed as

$$K_\gamma = \frac{2}{1-\left(\frac{R_{IC}}{R_{IB}}\right)^2} \quad [4.10]$$

The Reynolds number (Re) was calculated for the inner chamber of the double Couette cell using the following equation

$$Re = \frac{\theta R_{IC}\left(R_{IB} - R_{IC}\right)}{\nu} \quad [4.11]$$

where ν is the kinematic viscosity of sample solutions (m^2/s)

Using the Double Couette cell, the turbulence transition in the inner chamber occurs at Re ~ 1000. Thus, all rheological measurements in our study were taken well above this Re value.

4.4 Results and Discussion

4.4.1 Characterization of PEO in Aqueous Solutions

PEO of different molecular weights in aqueous solution were characterized by viscometric and light scattering techniques at 30°C. Table 4.1 lists the intrinsic viscosities, $[\eta]$, and Huggins coefficients, k_H, of aqueous PEO solutions at 30°C. Uncertainties indicate errors obtained from repeated measurements of the same samples. The corresponding viscosity-average molecular weights are quite close to the manufacturer quoted values, with the exception of PEO20, for which the measured M_v is lower by a factor of two from the quoted value. This may indicate that the high-end portion of the molecular weight distribution was cut off during the filtration of solutions prior to experimental analysis. The Huggins coefficient varies between 0.26 and 0.37. These are typical values for flexible polymer chains in good solvents [26]. The agreement between the measured and specified M_v suggests that the prepared aqueous PEO solutions do not contain PEO aggregates.

Table 4.2 shows physical parameters obtained from static and dynamic light scattering measurements of aqueous PEO solutions of various molecular weights. The average weight molecular weights, M_w, obtained from the static light scattering measurements are comparable to the viscosity molecular weights in Table 4.1 and to previously published data [24], and thus confirm that the true molecular weight of PEO20 is approximately 18.0×10^5 g/mol. The radius of gyration, R_g, varies with molecular weight as expected; from a low value of 54.2 nm for PEO1, to a high value of 110.2 nm for PEO20. These values are comparable to previously published results [25]. The second virial coefficient, A_2, varies between 0.5×10^{-4} to 4.3×10^{-4} mL mol/g^2, which are consistent with those of flexible polymers in good solvents [25]. From the dynamic light scattering measurements, the diffusion coefficients, D_o, of PEO and hydrodynamic radii, R_h, listed in Table 2 are also consistent with

literature values [24]. The corresponding R_g/R_h varies from 3.25 for PEO1 to 1.57 for PEO20, consistent with previously published data [29]. Hydrodynamic theory [30] predicts $R_g/R_h \approx 1.50$ for a linear flexible chain in good solvent, and $R_g/R_h \approx 1.2 - 1.3$ for theta solvent. Here, we point out that the normalized second cumulant, $\mu_2/\bar{\Gamma}^2$, systematically decreases from 0.50 to 0.32 with increasing molecular weight, consistent with previously published data [25]. Since $\mu_2/\bar{\Gamma}^2$ is a measure of the variance of the size distribution, these results indicate that our PEO samples are highly polydisperse and that the polydispersity is higher for the lower molecular weight samples. The higher values of R_g/R_h at lower molecular weights reflect the fact that these PEO samples have substantially wider molecular weight distributions.

Finally, we obtain a correlation between D_o and M_w: The scaling exponent a and the prefactor k found are 0.50 and 3.822×10^{-9} m^2/s, respectively. It is noted that the variation of a should satisfy $a \sim 0.6$ for flexible chains in good solvents [24,28]. The small value of a is again a consequence of the fact that the lower molecular weight PEO samples have higher polydispersities.

4.4.2 Characterization of Aqueous PEO/HTAC Solutions

The results from conductivity and surface tension measurements on aqueous HTAC and PEO/HTAC solutions at 30°C are summarized in Table 4.3. The critical micelle concentration, CMC, the surfactant concentration at which formation of micelles occurs, is 1.30 mM for the aqueous HTAC solution. This value is very consistent with the data of previous studies [24,31]. The interaction between PEO and HTAC was investigated by varying HTAC concentration, PEO concentration and molecular weight. The term CAC indicates the critical aggregate concentration, at which surfactant micelles bound to the polymer are formed. The CAC found in PEO solutions of different concentrations varies statistically from 0.19 to 0.22 mM via conductivity measurements, and from 0.18 to 0.20 mM via surface tension measurements. Thus, we find the CAC is independent of molecular weight and PEO concentration, consistent with a previous conclusion by Jones [32] that the CAC

value is only a function of polymer type. Likewise, in the case of PEO/SDS mixtures, independence of CAC over a wide range of PEO molecular weight was reported by Francois et al. [33]. For the PEO/HTAC systems studied here, a CMC transition is also observed at higher HTAC concentration, and is observed to slightly increase with increase of PEO concentration (Table 4.3). The data from conductivity measurements are consistent with those of surface tension measurements, and are in good agreement with results of Cockbain [34]. An increase in polymer concentration requires a greater amount of surfactant molecules to bind to the polymer chains at saturation, and consequently a greater concentration of surfactant molecules is required to form free micelles.

To identify the maximum binding concentration, MBC, of HTAC on PEO, viscometric measurements were carried out at high PEO concentrations, i.e., c_{PEO} = 1000 ppm for PEO $M_w = 0.91 \times 10^5$ and 6.06×10^5 g/mol and c_{PEO} = 500 ppm for 17.9×10^5 g/mol to locate the viscosity maximum which occurs when the PEO chains are saturated with surfactant. We then calculated the mole ratios of bound HTAC per EO repeat unit at the maximum binding concentration. The results indicate binding ratios of 0.40 mole of HTAC per mole of EO for $M_w = 0.91 \times 10^5$ g/mol, 0.22 mole of HTAC per mole of EO for $M_w = 6.06 \times 10^5$ g/mol, and 0.18 mole of HTAC per mole of EO for $M_w = 17.9 \times 10^5$ g/mol. These data are consistent with previous findings [24]; i.e., the mole ratio increases with increasing PEO concentration but decreases with increasing molecular weight. The corresponding calculated MBC values for the drag-reducing PEO solutions containing HTAC used in the present study are listed in Table 3. Note that the calculated MBC values of aqueous HTAC/PEO systems must be equal to or higher than CAC. Thus, for the system HTAC/PEO20_15, the PEO concentration is low enough that, when the CAC is reached, all PEO chains are saturated with bound HTAC micelles. Hence the calculated MBC (0.06 mM) is smaller than the CAC (0.18 mM), and we set the MBC = 0.18 mM (Table 4.3).

4.4.3 Turbulent Wall Shear Stress of Aqueous PEO Solutions

In our experimental work, all wall shear stress measurements were carried out using a double couette cell and a single couette cell, and temperature was fixed at

30°C. The onset of turbulence occurs at a critical Reynolds number, $Re_c \approx 1{,}000$ (≡ shear rate, $\dot{\gamma} = 68.29\ s^{-1}$). The correlation between friction factor, f, and Re follows a power law consisting of two regimes: with a scaling exponent of –1.0 corresponding to laminar flow, and a scaling exponent of –0.8 corresponding to turbulent flow. Our observations are in qualitative agreement with the previous published data done by Walowit et al. [35] who found Re_c at approximately 1,600. It is expected that some degradation of PEO may occur on prolonged or repeated exposure to turbulent flow. To avoid such complications, each drag reduction experiment was carried out with fresh samples and the duration of each experiment was kept short, about 10-11 minutes. In some experiments, we remeasured the torque vs. shear rate relation after a drag reduction run and found it be unchanged. We conclude that mechanical degradation, if present, does not affect our results significantly. Also, we do not feel solvent evaporation is a factor on these drag reduction experiments on highly dilute PEO solutions. The sample temperature was fixed at 30 °C and the room temperature was about 27 °C. The sample volume was about 50 mL having a contact area with air of about 5-7 cm^2. After each measurement, we did not observe any volume change in the loaded specimen.

Figures 4.1a-4.1e illustrate the dependence of wall shear stress, τ_w, on PEO concentration measured from aqueous solutions of different PEO molecular weights at Re 2500 and Re 5000 and 30°C. Figure 1a indicates no drag reduction takes place for PEO of molecular weight at or below 0.91×10^5 g/mol. This result may be compared with the study by Choi and Jhon [36] who observed, in a rotating disk apparatus, that the lowest molecular weight at which PEO solutions show drag reduction is $M_w = 2.65 \times 10^5$ g/mol. The cutoff molecular weight is expected to differ depending on polymer type and flow geometry. The wall shear stress data for higher molecular weight PEO are shown in Figures 4.1b – 4.1e. At a fixed Reynolds number, the wall shear stress decreases to a minimum value (maximum drag reduction) at a PEO concentration defined as the optimum concentration, c^*_{PEO}. The values of c^*_{PEO} are 50, 40, 30, and 15 ppm for PEO3 ($M_w = 3.04 \times 10^5$ g/mol), PEO6 ($M_w = 6.06 \times 10^5$ g/mol), PEO9 ($M_w = 8.03 \times 10^5$ g/mol) and PEO20 ($M_w = 17.9 \times 10^5$ g/mol), respectively. These results indicate that the optimum concentration, c^*_{PEO},

required for maximum drag reduction decreases with increasing molecular weight.

Figure 4.2 replots the data of Figure 1 as %DR versus c[η]. In Figure 4.2a, for Re = 2500, and Figure 4.2b for Re = 5000, we see that the data approximately superpose. The maximum drag reduction, for PEO6, PEO9, and PEO20, occurs at a polymer volume fraction of approximately $c^*_{PEO}[\eta] \sim 0.0145 \pm 0.002$ where c^*_{PEO} is the optimum PEO concentration. For PEO3, maximum drag reduction appears to locate at a slightly lower value, $c^*_{PEO}[\eta] \sim 0.0125$. This may reflect that PEO3 has substantially higher polydispersity than the PEO of higher molecular weight. No drag reduction occurs with PEO1 ($M_w = 0.91 \times 10^5$ g/mol), and its data are not shown in these figures. We note that the $c^*_{PEO}[\eta]$ value for each PEO molecular weight is two orders of magnitude smaller than the overlap value, $c_{PEO} \sim 1/[\eta]$. The percentage of maximum drag reduction increases with increasing PEO% for PEO M_w equal to 3.04 x 10^5, 6.06×10^5, 8.03×10^5, and 17.9×10^5 g/mol, respecti molecular weight, i.e., %DR is 24, 68, 83, and 85vely. These observations are generally consistent with previous observations of PEO solutions [37], and also consistent with either the viscometric [11-14] or elastic [15,16] theories of drag reduction. Beyond the $c^*_{PEO}[\eta]$, %DR decreases with increasing PEO concentration. This is possibly due to the increase in polymer concentration leading to interchain interactions, and the increase in shear viscosity which overwhelms the drag reduction effect.

4.4.4 Turbulent Wall Shear Stress of Aqueous HTAC Solutions

An experimental study of drag reduction of aqueous solutions of HTAC was carried out at 30°C. Figure 4.3 illustrates the dependence of wall shear stress, τ_w, on HTAC concentration ranging from 0 to 5 mM, at Reynolds number equal to 5000. At low HTAC concentrations, the wall shear stress decreases with increasing concentration up to the optimum concentration, c^*_{HTAC} equal to 1.7 mM, where we found a maximum drag reduction of about 51%. At HTAC concentrations greater than c^*_{HTAC}, the dependence of the wall shear stress on HTAC concentration becomes negligible. This result may be contrasted with previous published data [38,39] on solutions of HTAC containing sodium salicylate, which indicate that, at

very low concentrations, the amount of drag reduction increases with concentration, and levels off at some concentration depending on the surfactant chemical composition. From Figure 4.3, a maximum drag reduction of 51% is obtained at 1.7 mM of HTAC. However, it should be noted that the CMC of HTAC occurs at approximately 1.3 mM; thus we are apparently seeing drag reduction prior to micelle formation. Much published data [40,41,42] indicate that the presence of thread-like micelles is required for a surfactant to be a drag reducer. Apparently, in the double Couette geometry, free surfactant can have an effect in reducing turbulent wall stress by some unknown mechanism, which may be related to lowering of surface tension. In this context, however, it may be relevant to note recent work [43], which indicates that minute amounts of cationic surfactant can induce changes in turbulence intensity. It was therefore speculated that strong mixed flows may favor micelle formation even for concentrations as small as 0.05 mM, and/or that advection in a closed system leads to concentration gradients such that surfactant concentrations much higher than the average may occur locally near the wall.

4.4.5 Turbulent Wall Shear Stress of Aqueous PEO/HTAC Solutions

Low Molecular Weight PEO

The dependence of wall shear stress, τ_w, on HTAC concentration was investigated in aqueous HTAC/PEO solutions at T = 30°C and Re = 5000. Figure 4.4 illustrates the dependence of τ_w, on HTAC concentration for aqueous HTAC/PEO solutions of PEO M_w 0.91×10^5 g/mol at 40 and 200 ppm; these two systems are designated HTAC/PEO1_40 and HTAC/PEO1_200, respectively. With increasing HTAC concentration, the wall shear stress of HTAC/PEO1_40 and HTAC/PEO1_200 decreases towards a minimum value at the optimum concentrations, $c^*_{HTAC/PEO}$, ≈ 0.4 and 1.3 mM, respectively. The corresponding wall shear stresses are reduced in magnitude by 47 and 43%, respectively. Above $c^*_{HTAC/PEO}$, the wall shear stress increases towards a constant value at HTAC concentrations values close to the respective CMC values; i.e., 1.65 and 1.90 mM for

HTAC/PEO1_40 and HTAC/PEO1_200, respectively. We recall that drag reduction does not occur for aqueous solutions of PEO of M_w equal to 0.91×10^5 g/mol in the absence of HTAC, as evident in Figure 4.1a. Thus, addition of small amounts of HTAC to a non-drag reducing PEO solution produces a net drag reduction of almost a factor of two.

Two possible mechanisms can explain the drag reduction produced by adding HTAC to PEO aqueous solutions. In the first scenario, unassociated HTAC molecules in HTAC/PEO mixtures may act to produce drag reduction as evidenced by the data of Figure 4.3. In the second scenario, which may coexist with the first, binding of HTAC molecules to PEO chains occurs, resulting in a chain expansion, and an increase in hydrodynamic volume. The latter conjecture is supported by the results of Figure 4.4, where we find that τ_w for PEO1_40 decreases precipitously on addition of small amounts of HTAC, and that, for both PEO1_40 and PEO1_200, the minimum value of τ_w occurs at a $c^*_{HTAC/PEO}$ value which is equal to or slightly smaller than the MBC or maximum binding concentration. The latter is defined as the concentration at which polymer chains are saturated with surfactant molecules; and hence the polymer chains are fully expanded due to electrostatic repulsions between bound surfactant molecules [24]. Consequently, the chain hydrodynamic radius, R_h and extensional viscosity increase to their maximum values at MBC. It is of particular interest that, for HTAC/PEO1_40, the wall stress decreases precipitously (greater than additivity) when exceedingly small amounts of HTAC are added, i.e. at levels below the CAC. This raises the possibility that the CAC is effectively reduced in turbulent flow, where the chains are stretched, or that the drag reducing action of free HTAC is somehow potentiated by the presence of PEO. Experiments on high molecular weight PEO at $c \sim c^*_{PEO}$ described below tend to favor the former interpretation. Above the MBC, R_h decreases, because the excess surfactant causes electrostatic screening between bound micelles, and therefore, chain contraction occurs. Our present results are consistent with this scenario in which we find that turbulent wall shear stress generally increases with HTAC concentration above the MBC.

High Molecular Weight PEO

Next we investigate the effect of surfactants on turbulent wall shear stress of aqueous PEO solution for PEO having molecular weights equal to $6.06x10^5$ and $17.9x10^5$ g/mol at identical concentration of 200 ppm (PEO6_200 and PEO20_200). This PEO concentration is well above c^*_{PEO}, the concentration at which wall shear stress is minimal. Figure 4.5 shows that on addition of HTAC, the wall shear stress decreases to minimum values at $c^*_{HTAC/PEO}$ = 0.8 and 1.0 mM for PEO6_200 and PEO20_200, respectively. It should be noted that these $c^*_{HTAC/PEO}$ values are approximately the same as the respective MBC values for these solutions. At $c^*_{HTAC/PEO}$, the wall shear stresses are reduced by nearly a factor of two. Above $c^*_{HTAC/PEO}$, the wall shear stress increases monotonically with increasing HTAC concentration. Thus, it appears possible that either or both of the mechanisms discussed above can explain the behaviors observed for the high molecular PEO, PEO concentrations above the c^*_{PEO}. However, it is pertinent to note that the drag reduction occurs at a PEO concentration where drag reduction is ineffective for PEO itself, due to interchain interactions. This appears to suggest that, in this case (see also the behavior of HTAC/PEO1_200), the effect is due to some influence of PEO/HTAC complex formation on interchain interactions, e.g. interchain structuring via electostatic interactions or interchain association of bound micelles.

Finally, we investigate turbulent wall shear stress upon addition of HTAC to solutions of PEO of molecular weights of $6.06x10^5$ and $17.9x10^5$ g/mol at the optimum PEO concentration or c^*_{PEO}. Figure 4.6 illustrates the dependence of wall shear stress, τ_w, on HTAC concentration for HTAC/PEO solutions of PEO molecular weight $6.06x10^5$ g/mol at 40 ppm (HTAC/PEO6_40) and HTAC/PEO solutions of PEO molecular weight $17.9x10^5$ g/mol at 15 ppm (HTAC/PEO20_15). Here, we find that wall shear stress for both systems monotonically increases with increasing HTAC concentration toward a nearly constant value when HTAC concentration approaches the respective CMC for each system; specifically, $CMC_{HTAC/PEO6\_40}$ = 1.70 mM and $CMC_{HTAC/PEO20\_15}$ = 1.80 mM. This behavior contrasts with the results for low molecular weight PEO, and high molecular weight PEO at concentrations

above c^*_{PEO}, where we find that adding surfactant initially reduces wall shear stress. To explain this surprising behavior, we first note that the loss of drag reduction effect occurs at very low added levels of HTAC, below the nominal CAC value. This appears to favor the interpretation, alluded to earlier, that the CAC is reduced in turbulent flow, since the effect of free HTAC is to decrease turbulent wall stress. We therefore deduce that the binding of HTAC to stretched PEO coils occurs in turbulent flow. In the case of PEO of molecular weight below that required for drag reduction effect, this confers drag reducing power through increase of hydrodynamic volume. In the case of high molecular weight PEO at c^*_{PEO}, this decreases drag reducing power by shifting the $c^*_{HTAC/PEO}$ to a value below c^*_{PEO}.

To confirm the latter, the change in wall stress was monitored while increasing PEO concentration in the presence of a fixed amount of HTAC, set at the MBC values for the PEO solutions studied in Fig. 4.6, viz, $MBC_{HTAC/PEO6\_40} = 0.2$ mM, and $MBC_{HTAC/PEO20\_15} = 0.18$ mM. The results are displayed in Figs. 4.7 and 4.8, respectively, and indeed confirm that the optimum concentration for drag reduction is lowered in the presence of HTAC. From Figs. 4.7 and 4.8, it is further apparent that the maximum % drag reduction is reduced in the presence of surfactant. Specifically, maximum drag reduction decreases from 68% to 50% for PEO6 and from 85% to 66% for PEO20. This suggests that the decrease in optimum concentration correlates with the increased hydrodynamic volume of the polymer surfactant complex, whereas the reduction in drag reducing efficiency may be connected to the increased rigidity of the complex. Finally, we note that at high PEO concentration, in Figs 4.7 and 4.8, τ_w decreases significantly in the presence of surfactant, consistent with the observation (Fig. 5) that binding of HTAC to PEO at PEO concentrations above c^*_{PEO} reduces wall stress.

4.5 Conclusions

We have investigated the turbulent wall shear stress of aqueous solutions of PEO, HTAC, and their mixtures at 30°C in Couette flow, at various PEO molecular weights and concentrations. In agreement with literature results, we find that higher molecular weights of PEO exhibit maximum drag reduction at lower optimum PEO

concentrations. There is a critical molecular weight of polymer where drag reduction does not occur. The optimal concentration for maximum drag reduction appears to scale inversely with polymer hydrodynamic volume. In dilute HTAC solutions, at concentrations below the CMC, we find turbulent wall shear stress diminishes significantly with HTAC concentration even though a threadlike micellar network structure does not exist in the quiescent solution. In aqueous HTAC/PEO mixtures, when the PEO molecular weight is below the critical value for drag reduction ($M_w = 0.91 \times 10^5$), binding of HTAC micelles induces drag reduction, presumably because of the accompanying increase in hydrodynamic volume of the complex. For solutions of high molecular weight PEO, M_w equal to 6.06×10^5 and 17.9×10^5 g/mol, at their optimum PEO concentrations for drag reduction, c^*_{PEO}, wall shear stresses increase with addition of HTAC, because the increase of hydrodynamic volume causes a shift of the optimum PEO concentration for drag reduction to lower values. Since this effect is seen at HTAC concentrations below the quiescent CAC, it appears that the CAC may be lowered in turbulent flow.

4.6 Acknowledgements

S. Suksamranchit would like to acknowledge the financial support from the Thailand Research Fund (TRF), the RGJ grant no. PHD/0149/2543. This work was financially supported by the fund from MTEC, grant no. MT-43-POL-09-144-G, and the fund from the ADB Consortium Grant. AMJ acknowledges financial support through NSF award DMR 0080114.

4.7 References

[1] W.M. Kulicke, M. Kotter, H. Grager, Adv Polym Sci. 89 (1989) 1.

[2] R.P. Singh, in N.P. Chermisinoff (Ed.), Encyclopedia of Fluid Mechanics, Vol. 9, Gulf Publishing, Houston, 1990, Chapter 14.

[3] R.A. Mostardi, L.C. Thomas, H.L. Green, F. VanEssen, R.F. Nokes, Biorheology. 15 (1978) 1.

[4] R.C.R. Figoeredo, E. Sabadini, Colloid and Surfaces A. 215 (2003) 77.

[5] H.L. Greene, R.F. Mostardi, R.F. Wokes, Polym. Eng. Sci. 20 (1980) 499.

[6] N.S. Berman, Ann. Rev. Fluid Mech. 10 (1978) 47.

[7] J.L. Zakin, D.L. Hunston, J Appl. Polym. Sci. 22 (1978) 1763.

[8] C.A. Kim, J.H. Sung, H.J. Choi, C.B. Kim, W. Chun, M.S. Jhon, J Chem Eng. Japan. 32 (1999) 803.

[9] P.S. Virk, AIChE J. 21 (1975) 625.

[10] B. Hlavacek, L.A. Rollin, H.P. Schreiber, Polymer. 17 (1976) 81.

[11] J.L. Lumley, Ann. Rev. Fluid Mech. 1 (1969) 367.

[12] J.L. Lumley, J. Polym. Sci. Macromolec. Rev. 7 (1973) 263.

[13] J.L. Lumley, Phys. Fluids. 20 (10) (1997) Pt II S64-S71.

[14] P.G. De Gennes, Physica. 140A (1986) 9.

[15] P.G. De Gennes, in A. Luigi (Ed), Introduction to polymer dynamics: An elastic theory of drag reduction, Cambridge University Press, Cambridge, Great Britain,1990, Chapter 4.

[16] G. Ryskin, Phys. Rev. Lett. 59 (18) (1987) 2059.

[17] B.A. Toms, Some observations on the flow of linear polymer solutions through straight tubes at large Reynolds numbers, in: Proceedings of the 1st International Congress of Rheology, vol. 2, North-Holland, Amsterdam, 1949, Section II, pp.135-141.

[18] R.C. Little, Ind. Eng. Chem. Fundam. 8 (1969) 557.

[19] L.C. Chou, Ph.D. Dissertation, The Ohio State University, Columbus, OH, 1991.

[20] B. Lu, Ph.D. Dissertation, The Ohio State University, Columbus, OH, 1997.

[21] B. Lu, X. Li, L.E. Scriven, H.T. Davis, Y. Talmon, J.L. Zakin, Langmuir. 14 (1998) 8.

[22] J. Myska, Z. Chara, Exp. Fluids. 30 (2) (2001) 229.

[23] J. Myska, Z. Lin, P. Stepanek, J.L. Zakin, J Non-Newtonian Fluid Mech. 97 (2001) 251.

[24] K.Y. Mya, A.M. Jameison, A. Sirivat A, Langmuir. 16 (2000) 6131.

[25] K.Y. Mya, A. Sirivat, A.M. Jamieson, Macromolecules. 34 (15) (2001) 5260.

[26] M. Stickler and N. Sutterlin, in J. Brandrup and E.H. Immergut (Eds.), Polymer Handbook, Concentration dependence of the viscosity of dilute polymer solutions:

Huggins and Schulz-Blaschke coefficients, 3rd edition, Vol. 2, A Wiley-Interscience Publication, New York, Chapter 7.

[27] W. Brown, J. Fundin, M.D. Miguel, Macromolecules. 26 (26) (1992) 7192.

[28] K. Devanand, J.C. Selser, Macromolecules. 24 (1991) 5943.

[29] Y. Kanbe, C. Honda, Polymer Communications. 25 (1984) 154.

[30] B.H. Zimm, J Chem. Phys. 24 (1956) 269.

[31] A.W. Rålton, D.N. Eggenberger, H.J. Harwood, P.L. Du Brow, J Am. Chem. Soc. 69 (9) (1947) 2095.

[32] M.N. Jones, J Colloid Interface Sci. 23 (1967) 36.

[33] J. Francois, J. Dayantis, J. Sabbadin, Eur. Polym. J. 21 (1985) 165.

[34] E.G. Cockbain , Trans Faraday Soc. 49 (1953) 104.

[35] J. Walowit, S. Tsao, R.C. Di Proma, Trans. Am. Soc. Mech. Eng. J Appl Mech. 31 (1964) 585.

[36] H.J. Choi, M.S. Jhon, Ind. Eng. Chem. 35 (1996) 2993.

[37] M.E. Cowan, R.G. Hester, C.L. McCormick, J. Appl. Polym. Sci. 82 (2001) 1211.

[38] Z. Chara, J.L. Zakin, M. Severa, J. Myska, Exp. Fluids. 16 (1993) 36.

[39] J. Myska, P. Stepanek, J.L. Zakin, Colloid Polym Sci. 275 (3) (1997) 254.

[40] B. Lu, X. Li, J.L. Zakin, Y. Talmon, J. Non-Newtonian Fluid Mech. 71 (1997) 59.

[41] B. Lu, Y Zheng, H. T. Davis, L.E. Scriven, Y. Talmon, J. L. Zakin, Rheol. Acta, 37 (1998) 528.

[42] Z. Lin, L.C. Chou, B. Lu, Y. Zheng, H.T. Davis, L.E. Scriven, Y. Talmon, J.L. Zakin, Rheol. Acta. 39 (2000) 354.

[43] K. Arora, R. Sureshkumar, M.P. Scheiner, J.L. Piper, Rheol. Acta. 41 (2002) 25.

Table 4.1 Viscosity data for aqueous PEO solutions at 30°C

Code	Quoted $M_v \times 10^{-5}$ (g/mol)	$M_v \times 10^{-5}$ (g/mol)	$[\eta]$ (l/g)	K_H
PEO1	1.00	1.01 ± 0.03	0.100 ± 0.002	0.27 ± 0.02
PEO3	3.00	3.18 ± 0.08	0.245 ± 0.005	0.28 ± 0.02
PEO6	6.00	6.19 ± 0.14	0.412 ± 0.007	0.37 ± 0.01
PEO9	9.00	8.00 ± 0.16	0.503 ± 0.008	0.26 ± 0.02
PEO20	40.00	18.10 ± 0.24	0.950 ± 0.010	0.31 ± 0.02

Table 4.2 Dynamic and static light scattering data for aqueous PEO solutions at 30°C

Code	$M_w \times 10^{-5}$ (g/mol)	R_g (nm)	$A_2 \times 10^4$ (mL.mol/g^2)	$D_o \times 10^{12}$ (m^2/sec)	R_h (nm)	R_g/R_h	$\frac{\mu_2}{\bar{\Gamma}^2}$
PEO1	0.91 ± 0.05	54.2 ± 6.81	0.8	13.3 ± 1.1	16.69 ± 1.4	3.25 ± 0.1	0.50 ± 0.03
PEO3	3.04 ± 0.34	74.4 ± 11.4	1.4	7.0 ± 0.8	31.71 ± 3.6	2.34 ± 0.1	0.49 ± 0.03
PEO6	6.06 ± 0.08	89.1 ± 6.32	0.9	5.7 ± 0.3	38.87 ± 2.2	2.29 ± 0.1	0.39 ± 0.05
PEO9	8.03 ± 0.61	92.3 ± 3.08	4.3	4.6 ± 0.4	48.56 ± 4.2	1.90 ± 0.1	0.37 ± 0.05
PEO20	17.90 ± 0.37	110.2 ± 18.1	0.5	3.2 ± 0.4	70.24 ± 9.3	1.57 ± 0.1	0.32 ± 0.05

Table 4.3 Conductivity and surface tension data for quiescent aqueous PEO/HTAC solutions at 30°C

Code	PEO M_w x 10^{-5} (g/mol)	[PEO] (ppm)	Conductivity		Surface Tension		Visosity Measurement		
			CAC[a] (mM)	CMC[b] (mM)	CAC (mM)	CMC (mM)	C_{PEO}[c] (ppm)	C_{HTAC}[d] (mM)	MBC[e] (mM)
HTAC	-	-	-	1.30	-	1.30	-	-	-
HTAC/PEO1_40	0.91 ± 0.05	40	0.19	1.60	0.18	1.65	1000	9.00	0.36
HTAC/PEO1_200	0.91 ± 0.05	200	0.20	1.75	0.19	1.90	1000	9.00	1.80
HTAC/PEO6_40	6.06 ± 0.08	40	0.19	1.65	0.18	1.70	1000	5.00	0.20
HTAC/PEO6_200	6.06 ± 0.08	200	0.21	1.80	0.19	1.95	1000	5.00	1.00
HTAC/PEO20_15	17.90 ± 0.37	15	0.22	1.70	0.18	1.80	500	2.00	0.18*
HTAC/PEO20_200	17.90 ± 0.37	200	0.22	1.98	0.20	2.00	500	2.00	0.80

CAC[a] = critical aggregate concentration

CMC[b] = critical micelle concentration

C_{PEO}[c] = actual PEO concentration used in finding actual maximum binding concentration

C_{HTAC}[d] = actual HTAC concentration used in finding actual maximum binding concentration

MBC[e] = calculated maximum binding concentration

*The calculated MBC is 0.06 mM which is well below CAC. Thus, MBC is determined from the CAC.

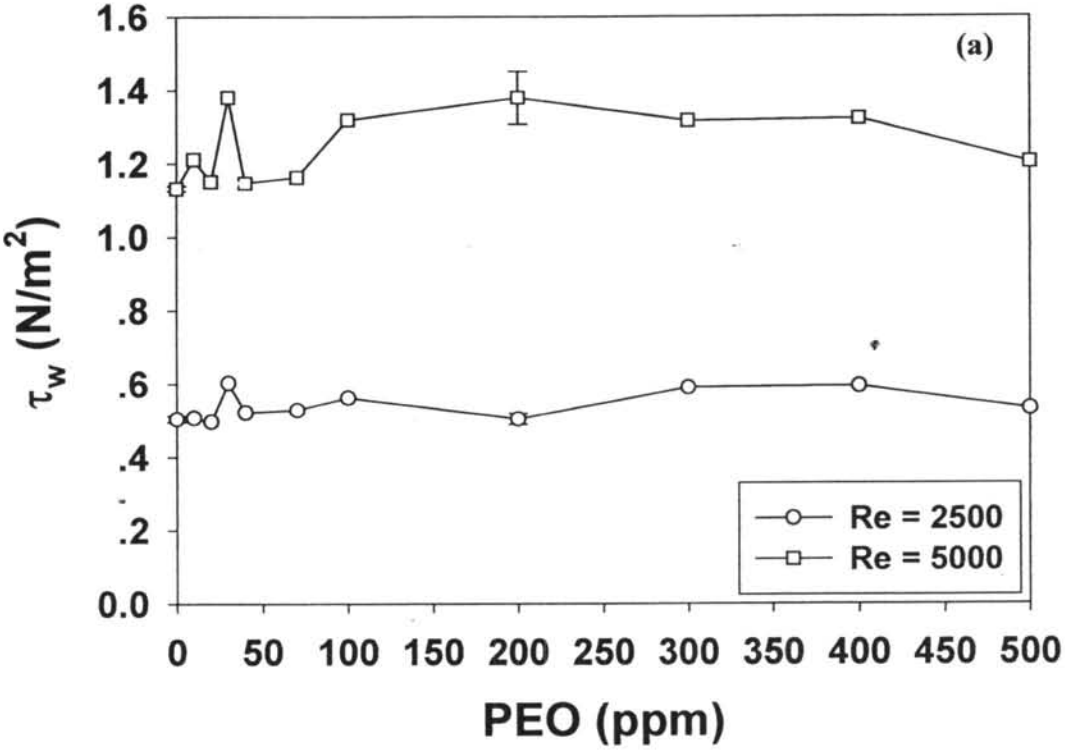
(a)
1.6
1.4
1.2
1.0
.8
.6
.4
.2
0.0
τ_w (N/m^2)
Re = 2500
Re = 5000
0 50 100 150 200 250 300 350 400 450 500
PEO (ppm)

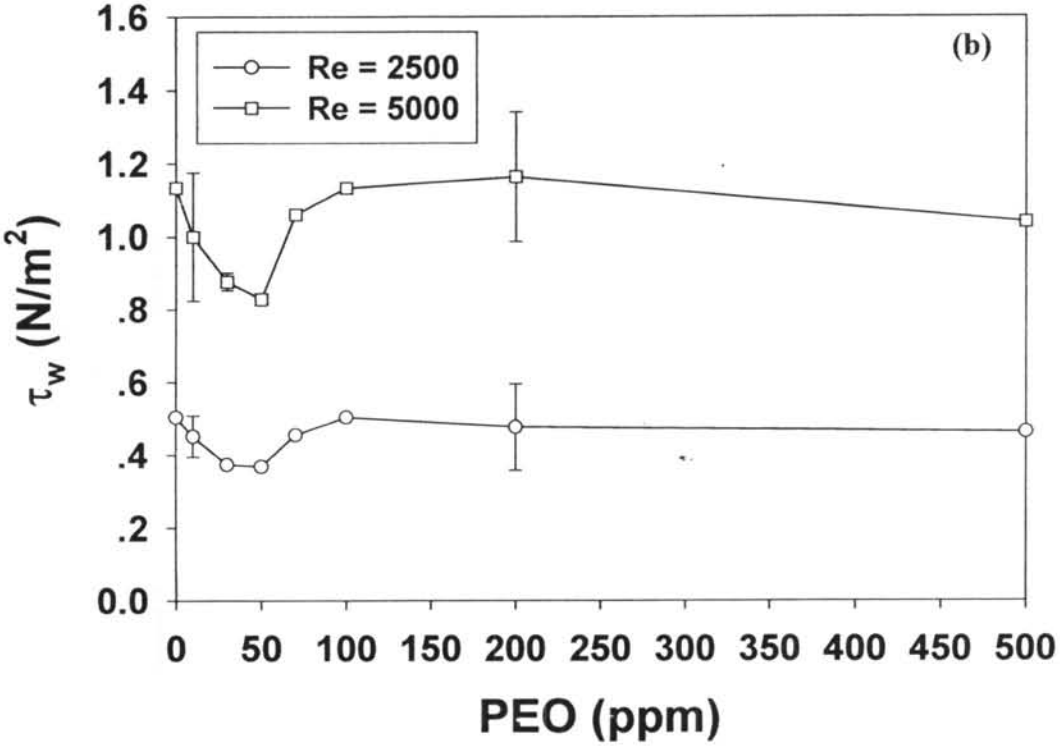
(b)
1.6
1.4
1.2
1.0
.8
.6
.4
.2
0.0
τ_w (N/m^2)
Re = 2500
Re = 5000
0 50 100 150 200 250 300 350 400 450 500
PEO (ppm)

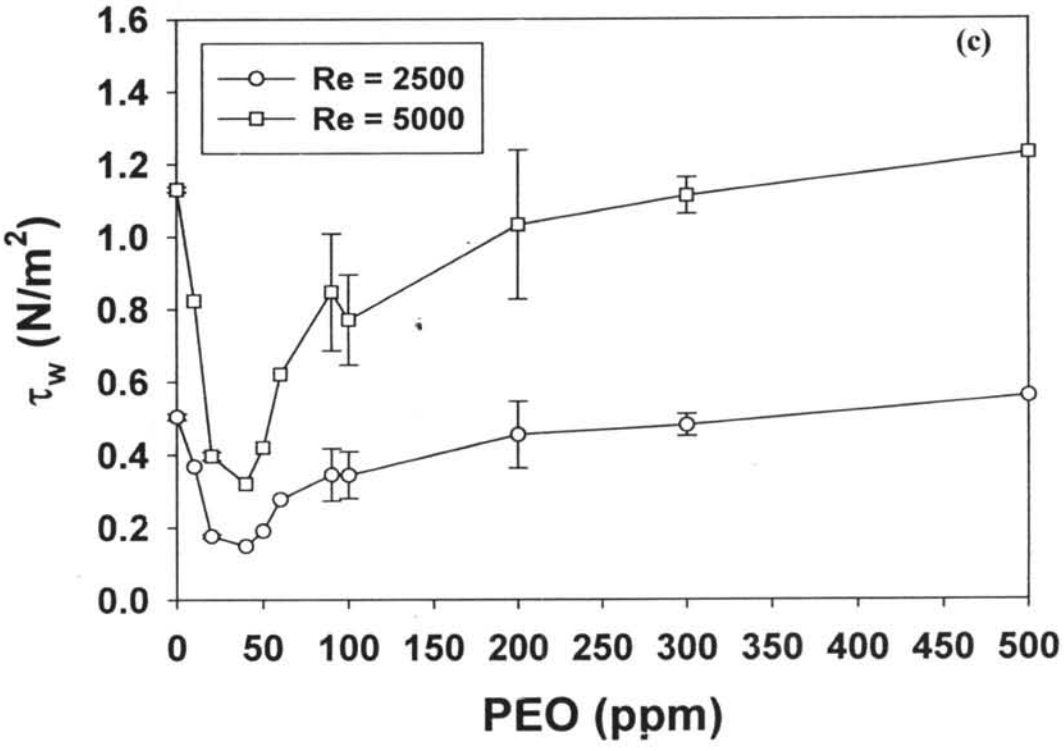
(c)
Re = 2500
Re = 5000
τ_w (N/m^2)
1.6
1.4
1.2
1.0
0.8
0.6
0.4
0.2
0.0
0
50
100
150
200
250
300
350
400
450
500
PEO (ppm)

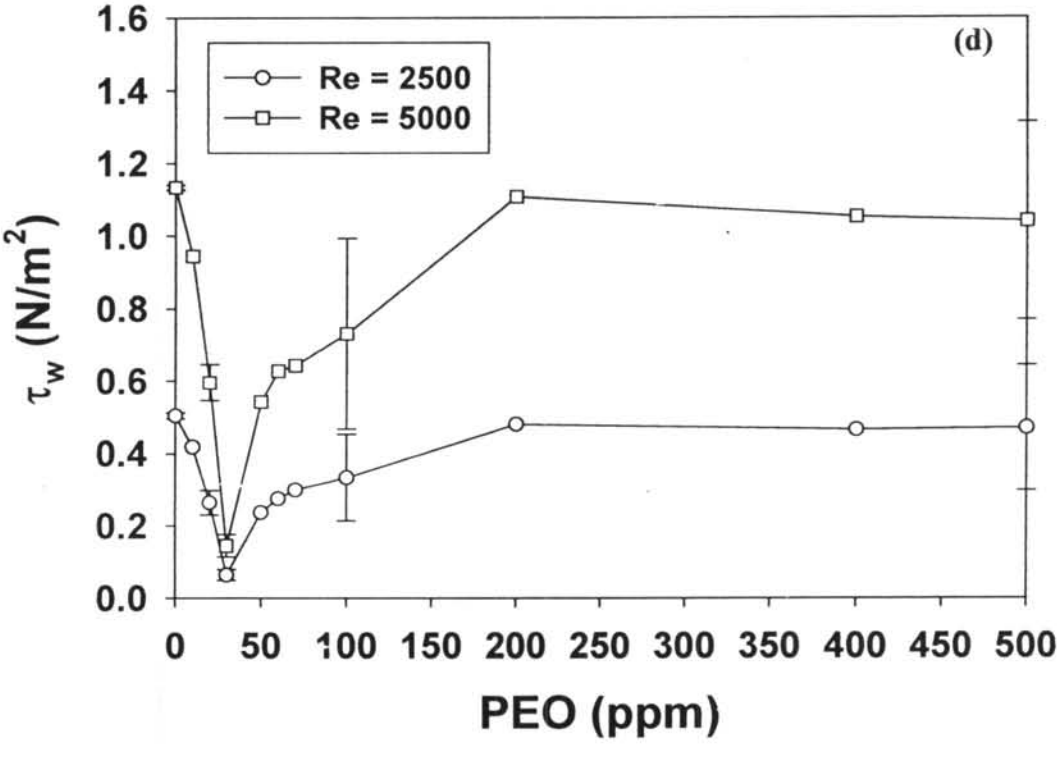
(d)
Re = 2500
Re = 5000
τ_w (N/m^2)
1.6
1.4
1.2
1.0
0.8
0.6
0.4
0.2
0.0
0
50
100
150
200
250
300
350
400
450
500
PEO (ppm)

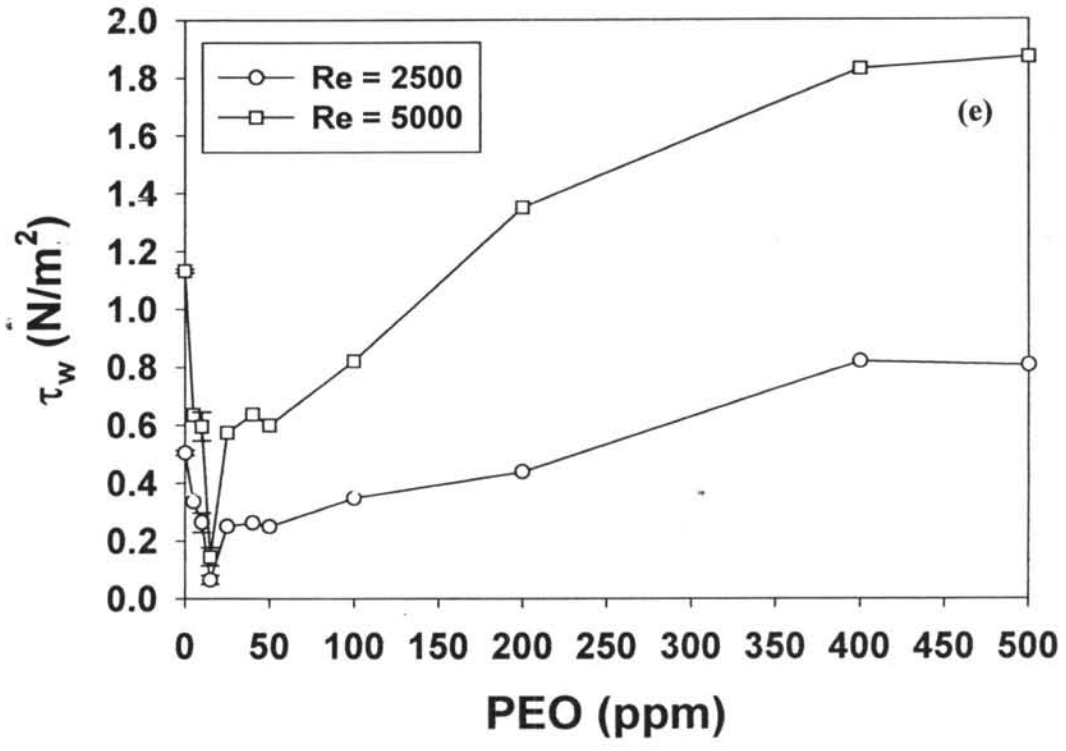

Figure 4.1 Dependence of wall shear stress, τ_w, on PEO concentrations for aqueous PEO solutions at 30°C, Re = 2500 and Re = 5000. **(a)** PEO1, $M_w = 0.91 \times 10^5$ g/mol; **(b)** PEO3, $M_w = 3.04 \times 10^5$ g/mol; **(c)** PEO6, $M_w = 6.06 \times 10^5$ g/mol; **(d)** PEO9, $M_w = 8.03 \times 10^5$ g/mol and **(e)** PEO20, $M_w = 17.9 \times 10^5$ g/mol.

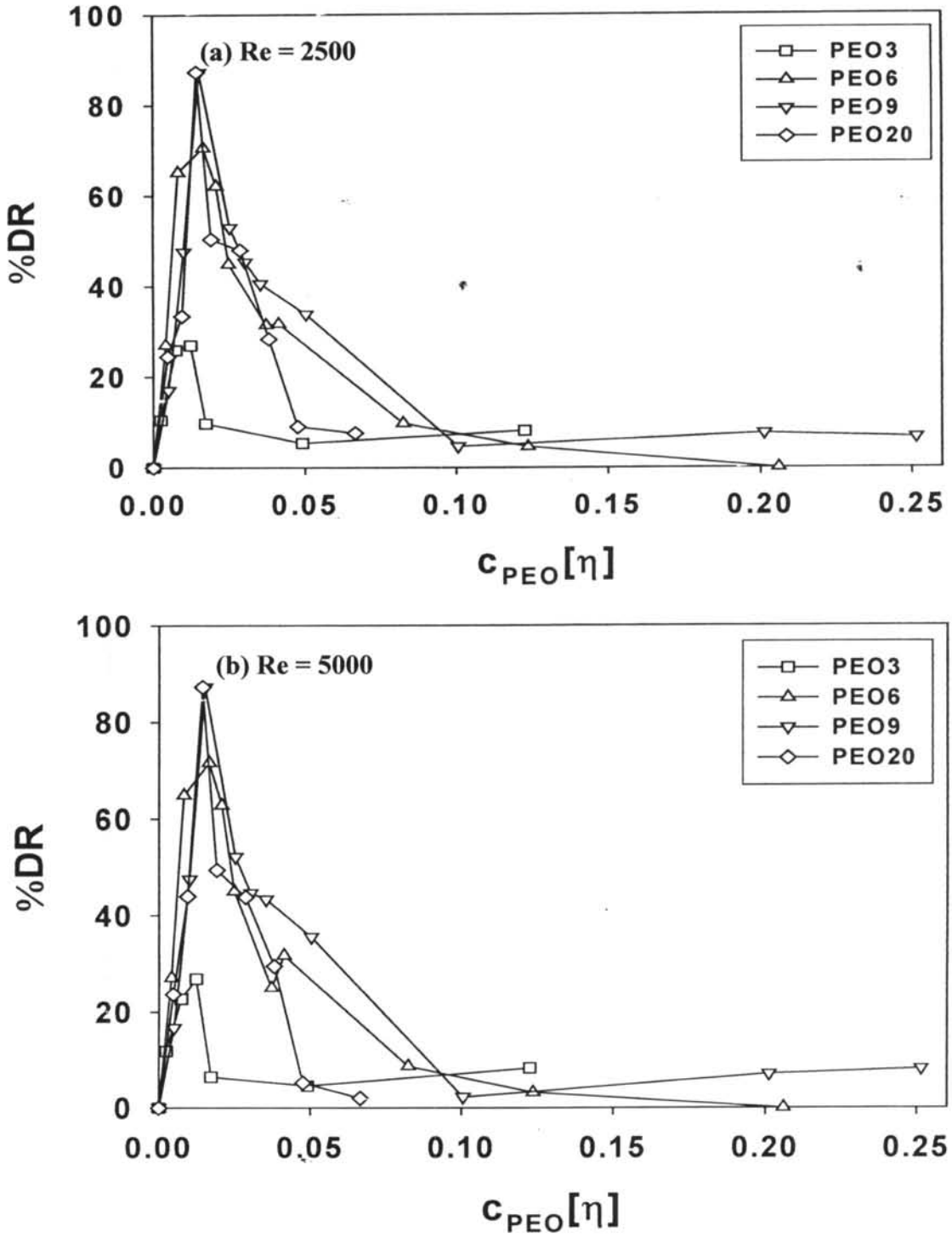

Figure 4.2 Plots of %DR versus c[η] of PEO in aqueous solutions at different concentrations and molecular weights at 30°C: **(a)** Re = 2500; and **(b)** Re = 5000, PEO3 = PEO $M_w = 3.04 \times 10^5$ g/mol; PEO6 = PEO $M_w = 6.06 \times 10^5$ g/mol; PEO9 = PEO $M_w = 8.03 \times 10^5$ g/mol and PEO20 = PEO $M_w = 17.9 \times 10^5$ g/mol.

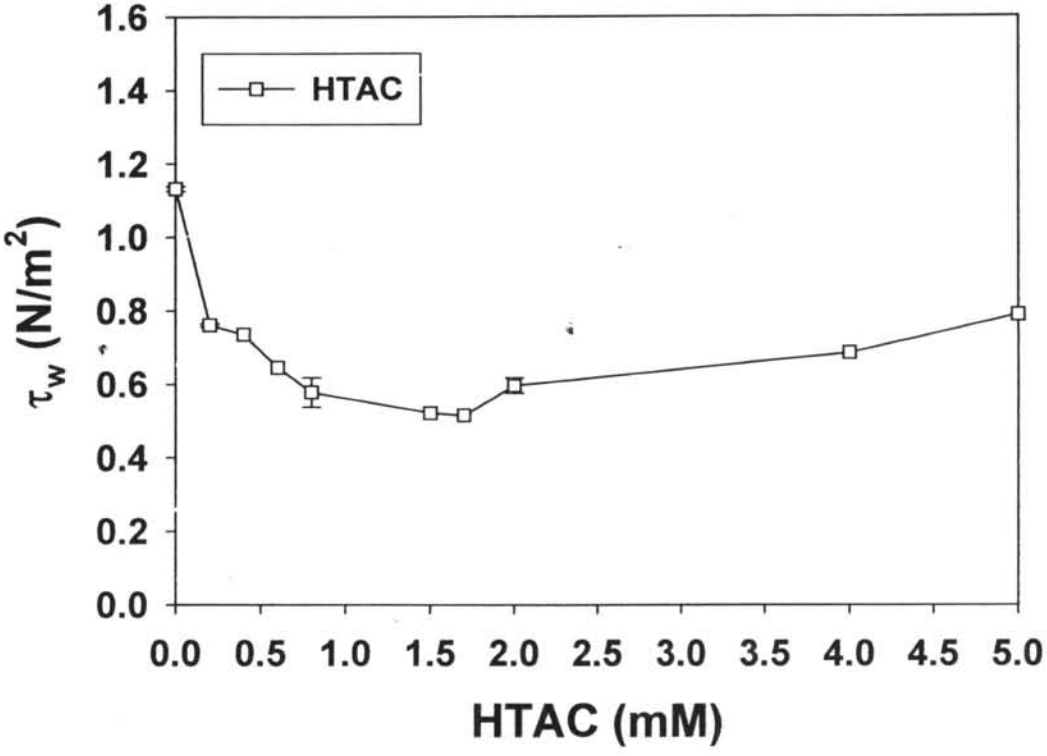

Figure 4.3 Dependence of wall shear stress, τ_w, on HTAC concentrations at 30°C for aqueous HTAC solutions at Re = 5000. *CMC_{HTAC} is 1.3 mM.

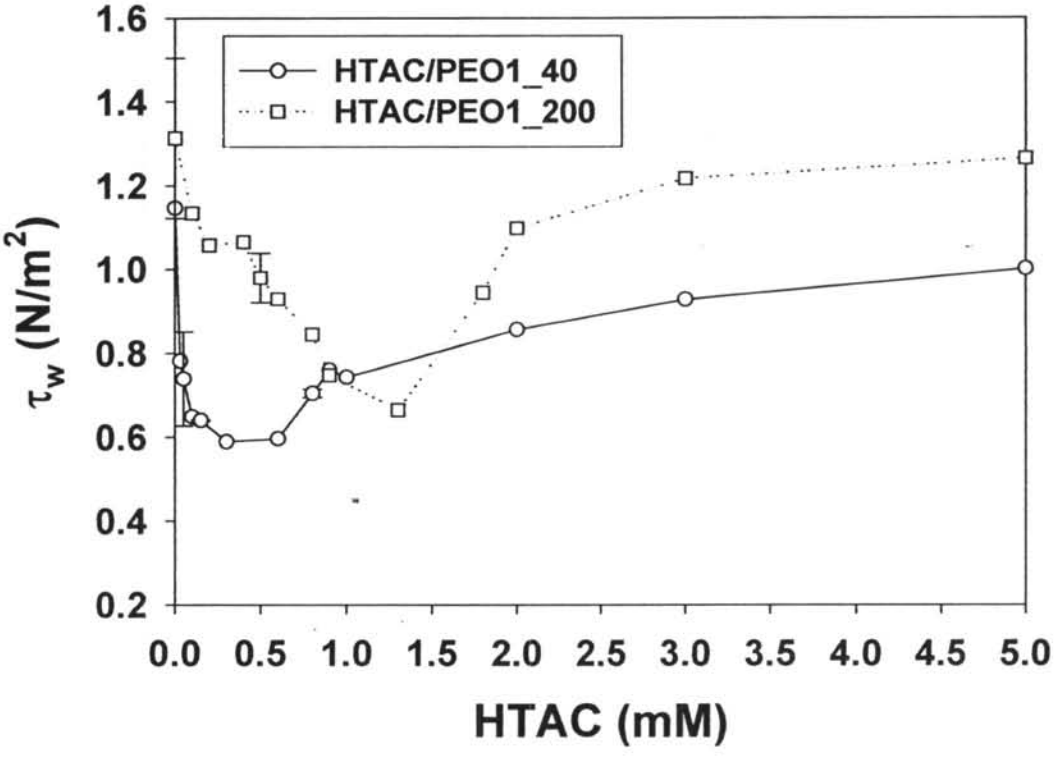

Figure 4.4 Dependence of wall shear stress, τ_w, on HTAC concentrations at 30 °C and Re =5000 for solutions of: **(a)** HTAC/PEO1_40, PEO $M_w = 0.91x10^5$ g/mol 40 ppm; **(b)** HTAC/PEO1_200, PEO $M_w = 0.91x10^5$ g/mol 200ppm. *MBC is maximum binding concentration of HTAC on PEO; $MBC_{HTAC/PEO1\_40}$ = 0.36 mM, $MBC_{HTAC/PEO1\_200}$ = 1.80 mM.

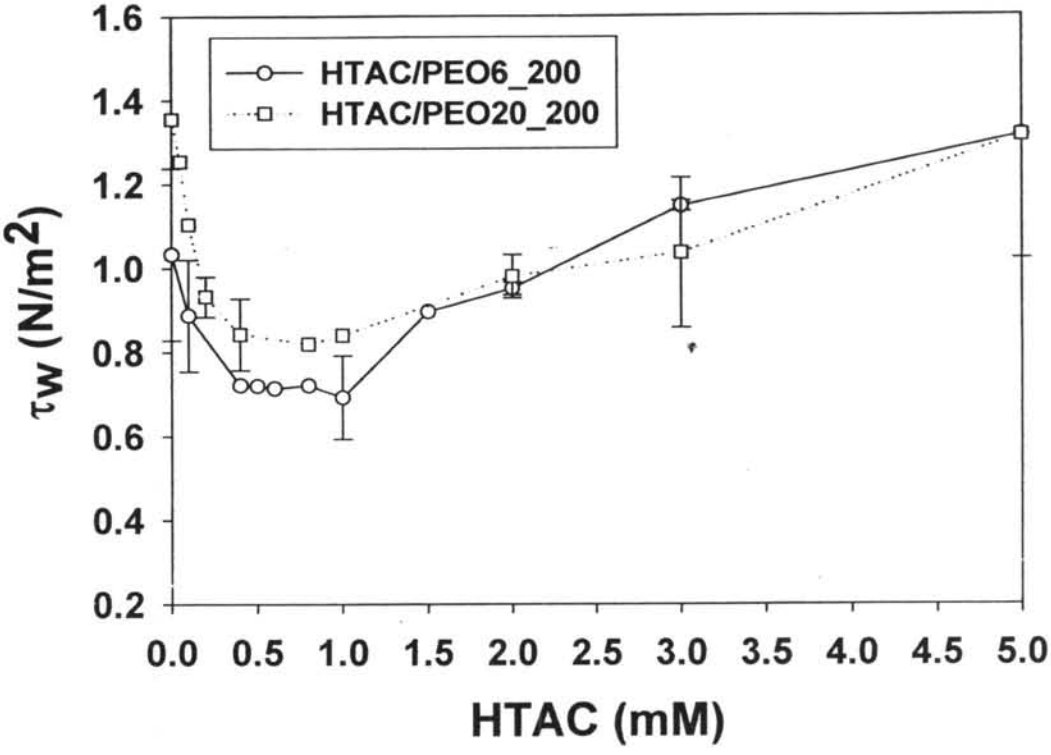

Figure 4.5 Dependence of wall shear stress, τ_w, on HTAC concentrations at 30 °C and Re = 5000 for solutions of: **(a)** HTAC/PEO6_200, PEO $M_w = 6.06 \times 10^5$ g/mol 200 ppm; **(b)** HTAC/PEO20_200, PEO $M_w = 17.9 \times 10^5$ g/mol 200 ppm. *MBC is maximum binding concentration of HTAC on PEO; $MBC_{HTAC/PEO6\_200}$ = 1.00 mM, $MBC_{HTAC/PEO20\_200}$ = 0.80 mM.

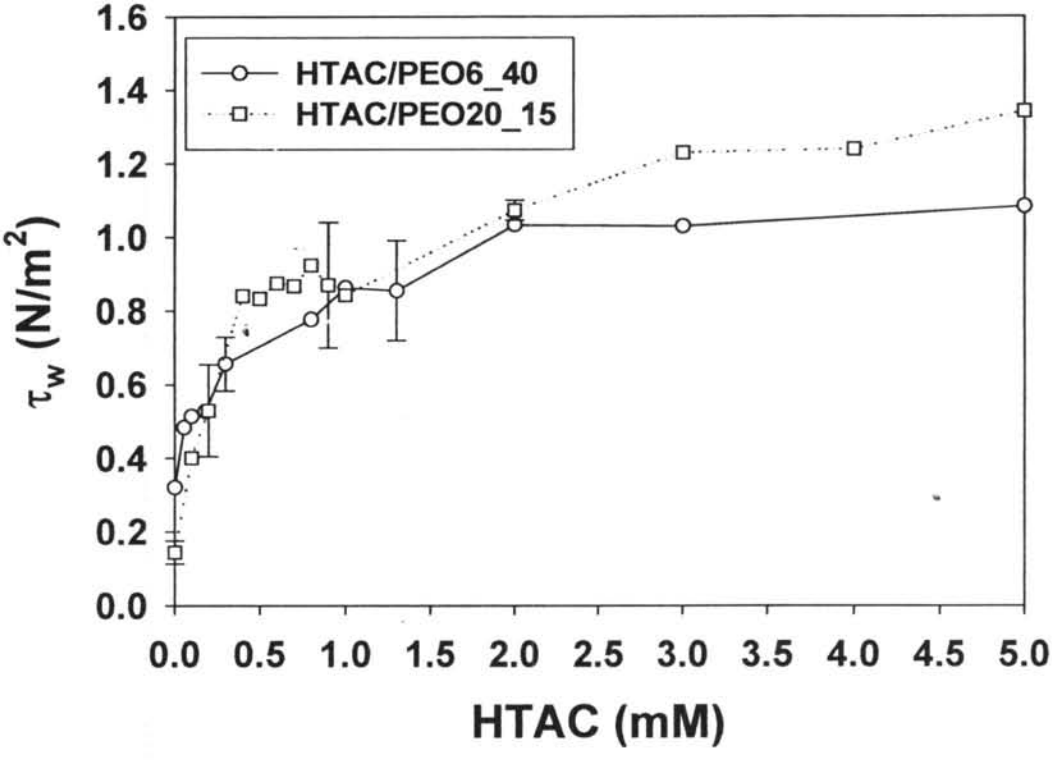

Figure 4.6 Dependence of wall shear stress, τ_w, on HTAC concentrations at 30 °C and Re = 5000 for solutions of: **(a)** HTAC/PEO6_40, PEO $M_w = 6.06 \times 10^5$ g/mol 40 ppm; **(b)** HTAC/PEO20_15, PEO $M_w = 17.9 \times 10^5$ g/mol 15 ppm. *MBC is maximum binding concentration of HTAC on PEO; $MBC_{HTAC/PEO6\_40}$ = 0.20 mM, $MBC_{HTAC/PEO20\_15}$ = 0.06 mM.

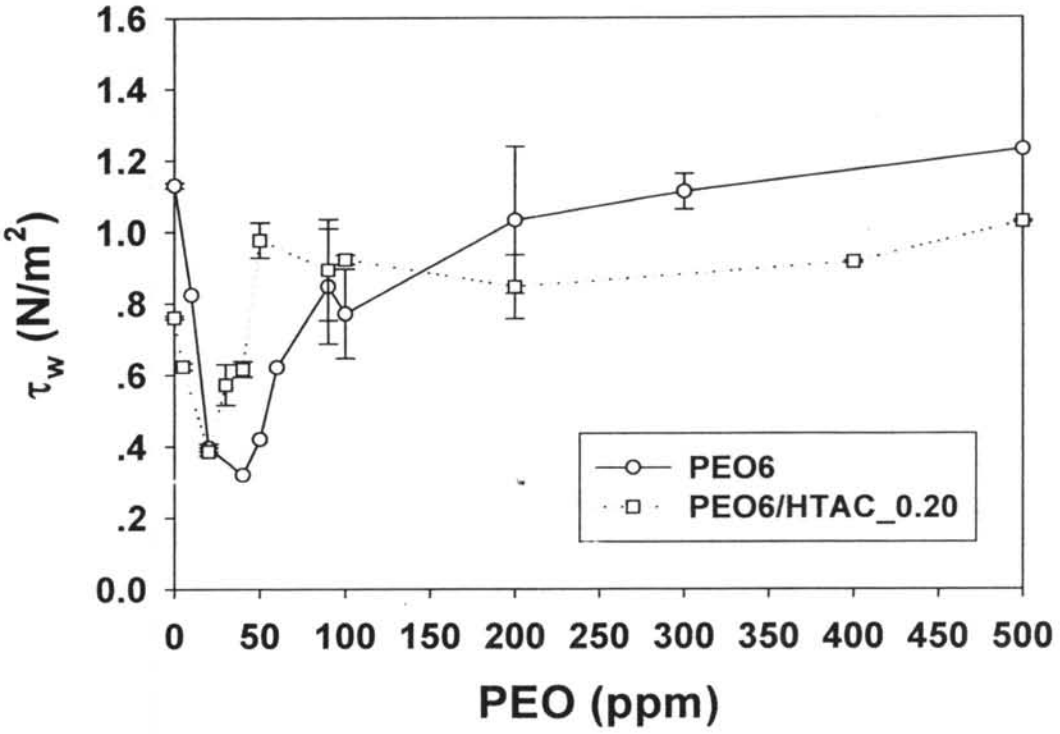

Figure 4.7 Dependence of wall shear stress, τ_w, on PEO concentrations at 30°C and Re = 5000 for aqueous solutions of: (a) PEO6, PEO $M_w = 6.06 \times 10^5$ g/mol; (b) PEO6/HTAC_0.20, PEO $M_w = 6.06 \times 10^5$ g/mol and HTAC at 0.20 mM. *MBC is maximum binding concentration of HTAC on PEO; $MBC_{HTAC/PEO6\_40}$ = 0.20 mM.

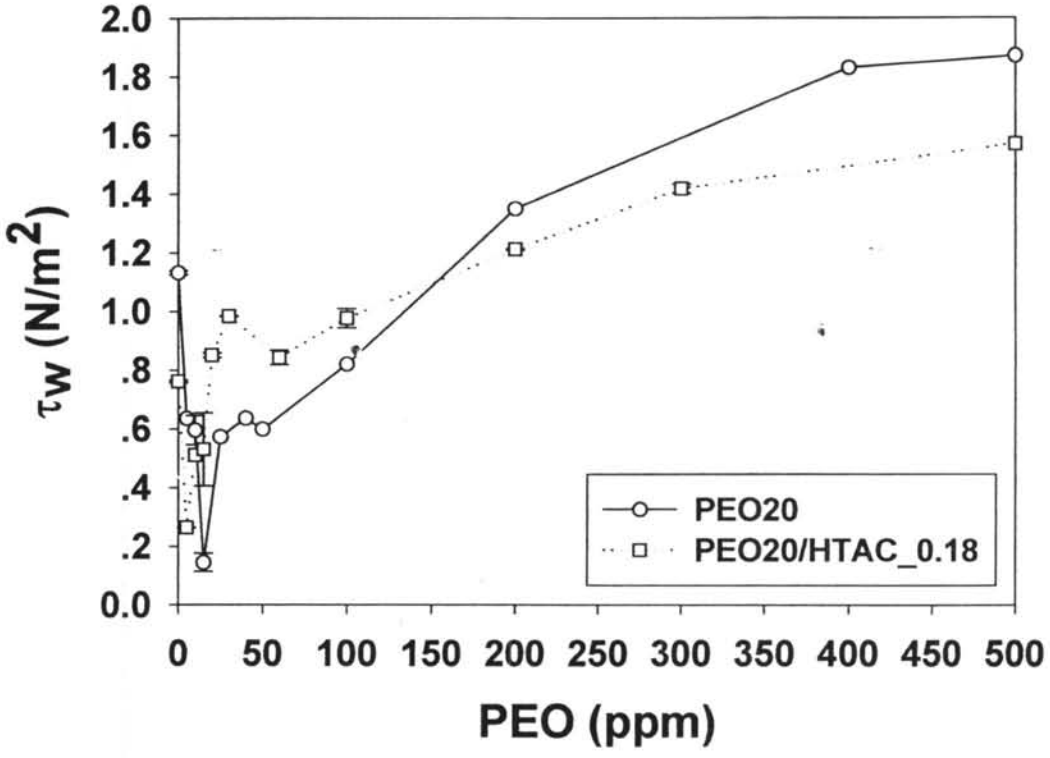

Figure 4.8 Dependence of wall shear stress, τ_w, on PEO concentrations at 30°C and Re = 5000 for aqueous solutions of: (a) PEO20, PEO $M_w = 17.9 \times 10^5$ g/mol; (b) PEO20/HTAC_0.18, PEO $M_w = 17.9 \times 10^5$ g/mol and HTAC 0.18 mM.
*MBC is maximum binding concentration of HTAC on PEO; $MBC_{HTAC/PEO20\_15}$ = 0.18 mM.